Sectorial Ganglion Cell Complex Thickness as Biomarker of Vision Outcome in Patients With Dominant Optic Atrophy

Marco Battista,[1] Catarina P. Coutinho,[2] Alessandro Berni,[1] Enrico Borrelli,[1] Alice Galzignato,[2] Giorgio Lari,[1] Lisa Checchin,[1] Irene C. Pizza,[1] Luigi Brotto,[3] Paolo Nucci,[3] Francesco Bandello,[1] Maria Lucia Cascavilla,[1] and Piero Barboni[1,2]

[1]Department of Ophthalmology, University Vita-Salute, IRCCS Ospedale San Raffaele, Milan, Italy
[2]Studio Oculistico d'Azeglio, Bologna, Italy
[3]Department of Clinical Science and Community Health, University of Milan, Milan, Italy

Correspondence: Piero Barboni, Department of Ophthalmology, University Vita-Salute San Raffaele, Via Olgettina 60, Milan 20054, Italy; p.barboni@studiodazeglio.it.

MLC and PB contributed equally to the work presented here and should therefore be regarded as equivalent authors.

Received: September 7, 2023
Accepted: December 4, 2023
Published: January 9, 2024

Citation: Battista M, Coutinho CP, Berni A, et al. Sectorial ganglion cell complex thickness as biomarker of vision outcome in patients with dominant optic atrophy. *Invest Ophthalmol Vis Sci.* 2024;65(1):24. https://doi.org/10.1167/iovs.65.1.24

Purpose. Dominant optic atrophy (DOA) is an inherited condition caused by autosomal dominant mutations involving the *OPA-1* gene. The aim of this study was to assess the relationship between macular ganglion cell and inner plexiform layer (GC-IPL) thickness obtained from structural optical coherence tomography (OCT) and visual outcomes in DOA patients.

Methods. The study recruited 33 patients with confirmed *OPA-1* heterozygous mutation and DOA. OCT scans were conducted to measure the GC-IPL thickness. The average and sectorial Early Treatment Diabetic Retinopathy Study (ETDRS) charts (six-sector macular analysis to enhance the topographical analysis) centered on the fovea were considered. Several regression analyses were carried out to investigate the associations between OCT metrics and final best-corrected visual acuity (BCVA) as the dependent variable.

Results. The mean BCVA was 0.43 ± 0.37 logMAR, and the average macular GC-IPL thickness was 43.65 ± 12.56 µm. All of the GC-IPL sectors were significantly reduced and correlated with BCVA. The univariate linear regression and the multivariate stepwise regression modeling showed that the strongest association with final BCVA was observed with the internal superior GC-IPL thickness. Dividing patients based on BCVA, we found a specific pattern. Specifically, in patients with BCVA $\leq$ 0.3 logMAR, the external superior and inferior sectors together with the internal superior were more significant; whereas, for BCVA > 0.3 logMAR, the external superior sector and internal superior sector were more significant.

Conclusions. The study identified OCT biomarkers associated with visual outcomes in DOA patients. Moreover, we assessed a specific OCT biomarker for DOA progression, ranging from patients in the early stages of disease with more preserved GC-IPL sectorial thickness to advanced stages with severe thinning.

Keywords: dominant optic atrophy, OCT, retinal ganglion cells

Dominant optic atrophy (DOA) is the most frequent hereditary optic neuropathy, with a prevalence of three cases per 100,000 individuals worldwide.[1] Approximately 70% of the affected patients present a pathogenic mutation in the *OPA-1* gene (3q28-q29), even though other mutations are commonly found in syndromic forms of the disease (*OPA-3*, *WFS-1*, *AFG3L2*, *NR2F1*).[2–5] The nuclear *OPA-1* gene encodes for a mitochondrial dynamin GTPase multifunctional protein connected with the mitochondrial activity, playing a critical role in the stabilization of mitochondrial cristae structure, mtDNA maintenance, respiratory chain efficiency, and cell calcium exchange management.[6] DOA mutations severely impair mitochondrial structure and function, ultimately leading to mitochondria fragmentation and a mitophagy rate increase. All body cells are affected in patients with DOA, but the resulting damage is only noticeable in specific tissues, such as retinal ganglion cells (RGCs) and optic nerve fibers, leading to optic atrophy. The most likely hypothesis is that the small parvocellular RGCs, which are very long and unmyelinated, have a high energy demand that strains the densely packed mitochondria, mostly concentrated in the area just before the lamina cribrosa.[7,8] The preferential involvement of the papillomacular bundle is a typical mitochondrial pattern due to the energetic disadvantage of small RGC axons.[9]

DOA typically presents with bilateral and symmetric visual loss associated with dyschromatopsia and central or cecocentral scotomas. The age of onset can vary, but most cases become evident during childhood or early adulthood. Visual symptoms may progress slowly over time, leading

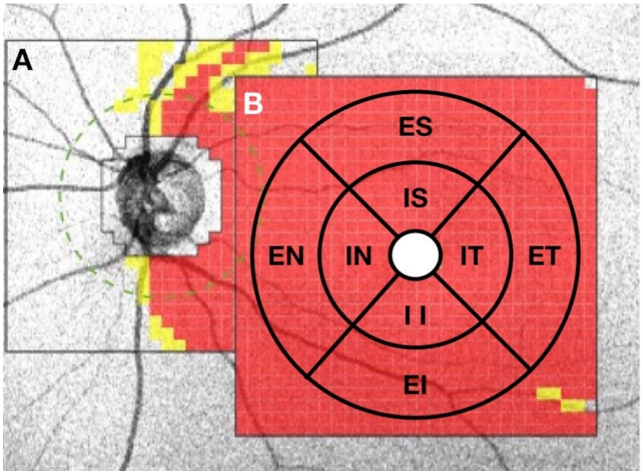

Figure 1. Limitations of the current OCT software analysis. The left eye of a patient affected by DOA shows temporal RNFL thinning (**A**) and diffuse GCL thinning (**B**). The ETDRS layout applied to the GCL analysis revealed deep and widespread damage in all sectors. IN, internal nasal; IS, internal superior; IT, internal temporal; II, internal inferior; EN, external nasal; ES, external superior; ET, external temporal; EI, external inferior.

to severe visual impairment in later stages of the disease. The structural changes may not always correlate directly with the severity of visual symptoms, leading to a perplexing clinical–structural disparity. Although some patients may exhibit severe optic nerve pallor, their visual symptoms might remain relatively mild.

Optical coherence tomography (OCT) provides essential data for the diagnostic management of the hereditary optic neuropathies and their differentials, enabling the measurement of retinal nerve fiber layer (RNFL) and RGC thickness. In particular, a previous study on DOA confirmed the preferential involvement of the papillomacular bundle and reported finding a significant reduction in the temporal and inferior RNFL quadrants.[10,11] The ganglion cell layer (GCL), defined as the sum of the retinal ganglion cell layer and inner plexiform layer (GC-IPL), was found to exhibit a sharp thickness reduction that progressively involves all of the macula sectors.[8–10]

In the context of GC-IPL thickness analysis, in advanced stages of the disease, the GC-IPL may become significantly thinner, potentially reaching the floor effect of the OCT, which means that the OCT machine may struggle to differentiate between extremely thin or absent ganglion cells, as the measurements approach the lower limits of the resolution of the device. As a result, the machine cannot provide precise measurements or distinguish subtle changes in thickness beyond a certain point (Fig. 1).

The variability of clinical expression and the structural discrepancy in DOA pose several challenges in the diagnosis and management of affected individuals. The aim of our study was to assess the relationship between OCT structural metrics and visual outcomes measurements in patients affected by DOA.

Methods

Patients with molecular diagnosis of *OPA-1* gene mutation were identified from the medical records of the neuro-ophthalmology department of San Raffaele Hospital, Milan, Italy. A cohort of healthy age-matched subjects served as the control group. The study adhered to the tenets of the Declaration of Helsinki and was approved by the San Raffaele Hospital Ethics Committee (143/INT/2020). Informed consent was obtained from all participants. To be included, patients and controls were required to have undergone a complete neuro-ophthalmological examination including measurement of best-corrected visual acuity (BCVA) using a Snellen chart assessment of visual acuity, slit-lamp biomicroscopy, intraocular pressure measurement, indirect ophthalmoscopy, and OCT. BCVA Snellen scores were converted to logMAR for the further analysis. Patient exclusion criteria included the presence of any retinal or optic nerve disease other than DOA and subjects with spherical or cylindrical refractive errors higher than 4 and 2 diopters, respectively. Finally, the presence of microcystic macular degeneration was verified in order to avoid errors in OCT segmentation.

Instrumentation and Procedures

All subjects underwent DRI OCT Triton (Topcon, Tokyo, Japan) measurement. Structural OCT volume scans of the macula (three-dimensional wide glaucoma module) were performed to measure macular GC-IPL thickness (Fig. 1). The average and sectorial Early Treatment Diabetic Retinopathy Study (ETDRS) charts centered on the fovea were considered for this analysis (Fig. 1). The ETDRS sectorial analysis was selected in order to achieve more specific information about topographical distribution from the central to peripheral GC-IPL (external superior, nasal, inferior, temporal and internal superior, nasal, inferior, and temporal) compared to the classical six-sector macular analysis (superior, superior/nasal, superior/temporal, inferior, inferior/nasal, and inferior/temporal).

Statistical Analysis

The statistical analysis was performed using the Statistical Functions module (spicy.stats) of Python 3.8. For the data distribution assessment, the Shapiro–Wilk test was used. If the data were normally distributed, a paired *t*-test was carried out for comparison of two samples; otherwise, the non-parametric Wilcoxon signed-rank test was used.

An univariate linear regression was performed to verify the correlation between BCVA and the thickness of the eight ETDRS GC-IPL sectors in patients with DOA. In order to identify significant groups of GC-IPL sectors related to BCVA and to highlight the most important ones, a multivariate stepwise regression analysis was carried out. To rule out the possible effect of considering both eyes of the same patient, linear mixed-effects model multivariate regression was also performed.

Moreover, we divided patients with DOA based on BCVA into two groups ($\leq$0.3 logMAR and >0.3 logMAR) in order to point out differences in disease progression and identify more specific biomarkers using univariate and multiple linear regression methods. $P < 0.05$ was considered significant. SHAP (SHapley Additive exPlanations) analysis was used to distinguish the importance of the different GC-IPL sectors when correlated to the BCVA using the different linear regression methods. To assess the sectorial thickness difference between control subjects and DOA patients, as well as how this difference varies among BCVA groups, the percentage change was calculated.

Investigative Ophthalmology & Visual Science

Results

A total of 66 eyes of 33 patients affected by DOA from 20 families with molecularly confirmed *OPA-1* gene mutation were identified (Table 1). The ratio of male to female was 20:13, and the mean age at the time of examinations was 32.1 ± 18.3 years old. The mean BCVA was 0.43 ± 0.37 logMAR, and the mean macular GC-IPL thickness was 43.65 ± 12.56 µm.

The comparative analysis among GC-IPL sectors (Table 2) showed that the internal superior sector was significantly thicker than all other sectors ($P < 0.001$), and the external inferior sector was thinner than the superior ($P < 0.001$) and temporal ($P = 0.009$) external sectors.

The univariate linear regression showed a correlation between BCVA and OCT metrics. All of the macular sectors were significantly reduced and correlated with BCVA (Table 3). The highest correlation with BCVA was found for the internal superior GC-IPL thickness ($R = -0.62$, $R^2 = 0.3908$, $P < 0.001$) (Fig. 2).

The multivariate stepwise regression modeling revealed that the most significant sectors were the internal nasal and superior and external superior, temporal, and inferior sectors (Table 4). Considering these sectors, the SHAP approach showed that the internal superior and external superior were the first and second most important sectors, respectively, for BCVA (Fig. 3). Furthermore, for the linear mixed-effects model, only the internal superior GC-IPL thickness was considered significantly correlated with BCVA (Table 5).

Dividing DOA patients based on BCVA into two groups of ≤0.3 logMAR (27 eyes) and >0.3 logMAR (39 eyes) and considering only the GC-IPL sectors that were statistically significant when employing the multivariate stepwise regression, we found a specific pattern through univariate regression analysis. For patients with BCVA ≤ 0.3 logMAR, the external superior, external inferior, external temporal, internal nasal, and internal superior sectors were significantly correlated with BCVA; whereas, for the group with BCVA > 0.3 logMAR, only the superior external and internal sectors were significantly correlated with BCVA (Table 6). Considering all of these sectors (external superior, inferior, and temporal and internal nasal and superior) together and

Table 1. Demographic Data

Demographic	
Patients/eyes, *n*	33/66
Pedigrees, *n*	20
Male, *n* (%)	20 (60.6)
Female, *n* (%)	13 (39.4)
Age at examination (y), mean ± SD	32.1 ± 18.3
BCVA (logMAR), mean ± SD	0.43 ± 0.37
Mutation classification (H/M), *n*	25/8

H, mutation causing haploinsuffiency; M, missense mutation.

Table 2. OCT Parameters for Patients With DOA

		Mean	SD	Minimum	Maximum
Internal (µm)	Nasal	44.82	14.94	23	87
	Superior	51.14	14.66	34	88
	Temporal	45.5	14.72	24	88
	Inferior	47.32	13.85	22	88
External (µm)	Nasal	43.06	9.22	21	71
	Superior	44.82	8.74	19	74
	Temporal	44.03	9.00	22	65
	Inferior	42.32	7.13	24	69

Table 3. Univariate Linear Regression Analysis for GC-IPL Sector Thicknesses and BCVA (in logMAR)

		R	R^2	*P*
Internal (µm)	Nasal	−0.48	0.2335	<0.001
	Superior	−0.62	0.3908	<0.001
	Temporal	−0.49	0.2412	<0.001
	Inferior	−0.48	0.2311	<0.001
External (µm)	Nasal	−0.47	0.2234	<0.001
	Superior	−0.59	0.3455	<0.001
	Temporal	−0.46	0.2009	<0.001
	Inferior	−0.43	0.1567	0.001

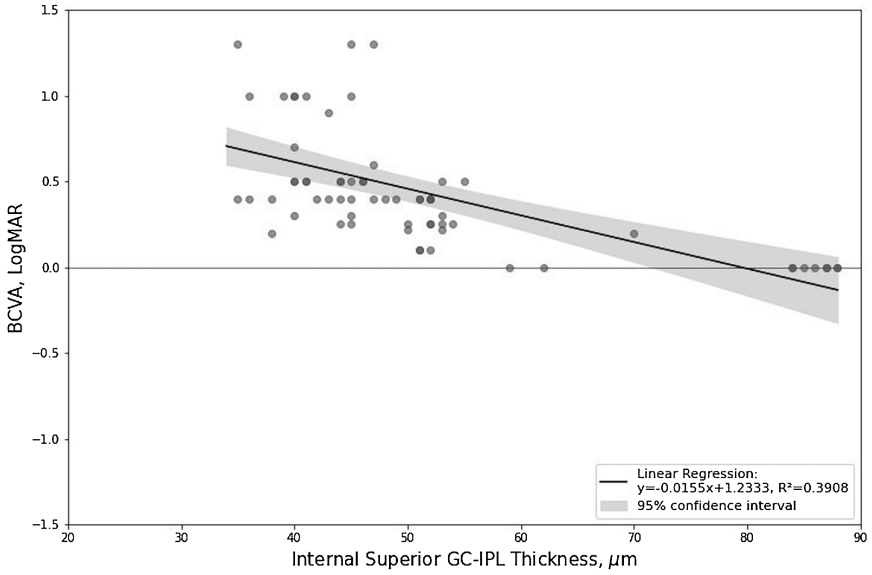

Figure 2. Univariate linear regression analysis of internal superior sector thickness and BCVA ($P < 0.001$).

Investigative Ophthalmology & Visual Science

Table 4. Multivariate Stepwise Regression Analysis for Statistically Significant GC-IPL Sectors Correlated to BCVA (in logMAR)

		Coefficient	*P*
Internal (µm)	Nasal	0.0143	0.006
	Superior	−0.0302	<0.001
External (µm)	Superior	−0.0462	<0.001
	Temporal	0.0213	0.003
	Inferior	0.0328	<0.001

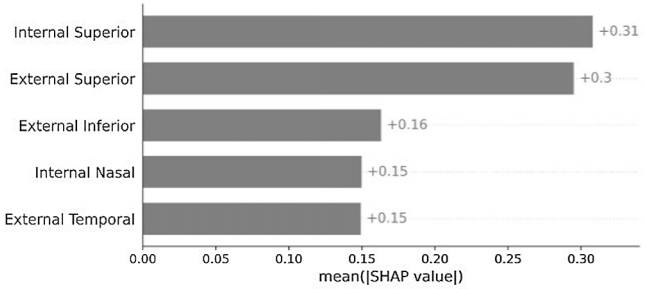

Figure 3. SHAP analysis for the statistically significant GC-IPL sectors when employing the multivariate stepwise regression considering all eyes.

Table 5. Linear Mixed-Effects Model Multivariate Regression for GC-IPL Sector Thickness and BCVA (in logMAR)

		Coefficient	*P*
Internal (µm)	Nasal	0.001	0.879
	Superior	−0.023	<0.001
	Temporal	0.004	0.409
	Inferior	0.001	0.744
External (µm)	Nasal	0.005	0.302
	Superior	−0.005	0.574
	Temporal	0.001	0.86
	Inferior	0.009	0.087

Table 6. Mean, SD, Minimum, and Maximum Thickness Values of GC-IPL Sectors for the Two BCVA Groups

						BCVA Correlation	
		Mean	SD	Min	Max	R^2	*P*
BCVA ≤ 0.3 logMAR (n = 27 eyes)							
Internal (µm)	Nasal	53.33	19.04	25	87	0.615	<0.001
	Superior	61.59	17.37	38	88	0.672	<0.001
External (µm)	Superior	50.07	7.78	37	74	0.297	0.0033
	Temporal	48.81	9.33	33	65	0.465	<0.001
	Inferior	46.04	7.46	33	69	0.248	0.0082
BCVA > 0.3 logMAR (n = 39 eyes)							
Internal (µm)	Nasal	38.92	6.83	23	52	0.008	0.594
	Superior	43.90	5.47	34	55	0.182	0.00675
External (µm)	Superior	41.18	7.48	19	54	0.150	0.0148
	Temporal	40.72	7.17	22	55	0.013	0.498
	Inferior	39.74	5.68	24	50	0.004	0.713

The BCVA correlation parameters refer to a univariate linear regression analysis.

applying a multivariate regression analysis, for the BCVA ≤ 0.3 logMAR group, the external inferior sector was statistically significant ($P = 0.017$) and was the most important one in the SHAP approach (Fig. 4); whereas, for the BCVA > 0.3 logMAR group, all of these sectors were statistically significant except the internal nasal ($P = 0.063$), which was also the less important in the SHAP analysis (Fig. 5). Considering the 68 eyes (34 patients) of the control group, the percentage

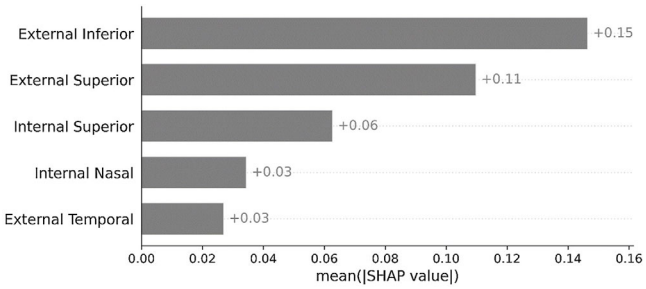

Figure 4. SHAP analysis for the statistically significant GC-IPL sectors when employing the multivariate stepwise regression for the group of eyes with a BCVA ≤ 0.3 logMAR.

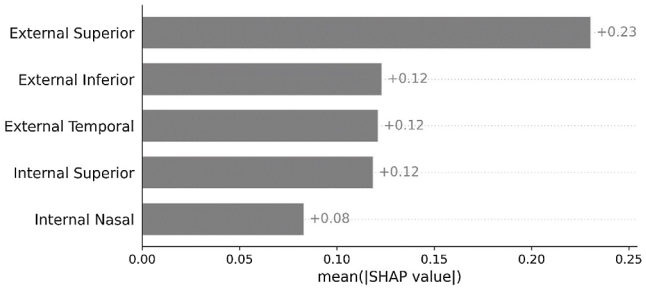

Figure 5. SHAP analysis for the statistically significant GC-IPL sectors when employing the multivariate stepwise regression for the group of eyes with a BCVA > 0.3 logMAR.

changes in sectorial thickness in comparison with patients with DOA are reported in Table 7.

Discussion

In this study, we focused on the structural impairment of GC-IPL thickness due to DOA-associated neural degeneration, and we found an overall thinning of the GC-IPL and a direct and proportionate correlation between the thickness of the superior parafoveal regions and the better visual acuity. The ETDRS macular analysis highlighted a difference between the internal and external GC-IPL thinning trend, as BCVA was correlated with the internal superior sector thickness and external superior, inferior, and temporal sector thicknesses. These data confirm two important hypotheses: (1) the early and preferential involvement of RGCs corresponds to small fibers of the papillomacular bundle (internal sectors) before subsequent involvement of other fibers of larger caliper (external sectors); second, GC-IPL thinning starts in the inferior nasal sectors of the macula and progressively deepens and enlarges in the other sectors at the same time.[10]

In our previous work, we showed that early severe thinning of the macular GC-IPL was correlated with the increasing severity of visual loss in DOA.[10] Moreover, the GC-IPL thinning preceded the RNFL damage at the disease onset, reflecting (1) preferential involvement of papillomacular fibers, with partial sparing of peripheral fibers, and (2) damage of RGC cellular bodies before the axonal degeneration. We concluded that the remaining peripapillary RNFL of the superior and nasal quadrants, corresponding to the temporal sectors (superior and inferior of the six-sector analysis) of the GC-IPL, was directly correlated with BCVA, as these central fibers were preserved for a longer

Investigative Ophthalmology & Visual Science

Table 7. Percentage Change With Respect to the Control Group for Each GC-IPL Sector Thickness

	Internal				External			
	Nasal	**Superior**	**Temporal**	**Inferior**	**Nasal**	**Superior**	**Temporal**	**Inferior**
Controls (µm)	93.1	94.5	88.9	93.3	71.9	67.0	70.0	63.9
DOA (µm)	44.8	51.1	45.5	47.3	43.1	44.8	44.0	42.3
Percent (%)	−51.8	−45.9	−48.8	−49.3	−40.1	−33.1	−37.0	−33.8
DOA, BCVA ≤ 0.3 logMAR (µm)	53.3	61.6	54.0	55.3	48.2	50.1	48.8	46.0
Percent (%)	−42.7	−34.8	−39.3	−40.7	−32.0	−25.2	−30.2	−27.9
DOA, BCVA > 0.3 logMAR (µm)	38.9	43.9	39.6	41.8	39.5	41.2	40.7	39.7
Percent (%)	−58.2	−52.8	−57.4	−55.1	−57.6	−55.7	−56.2	−57.3

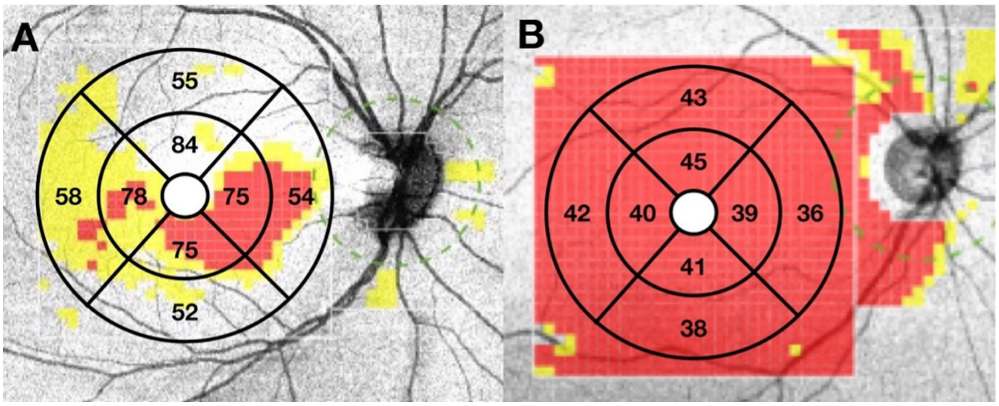

Figure 6. RNFL and GC-IPL thinning in DOA patients in the early (**A**) and advanced (**B**) stages.

time. However, the superior nasal and inferior nasal GC-IPL sectors, as well as the temporal RNFL quadrant corresponding to the papillomacular bundle, were the thinnest and most affected. Another study demonstrated the preferential involvement of inferior nasal and inferior sectors of the GC-IPL in DOA (six-sector analysis) which appeared more correlated to the BCVA progressive loss, while the superior temporal sectors (superior, superior temporal, and inferior) resulted thicker than the others, more correlated to the BCVA progressive loss.[12]

Recently, a correlation between BCVA and minimum GCL thickness in patients with Leber hereditary optic neuropathy (LHON) was reported. Furthermore, the capacity of this structural measurement as a predictor for visual prognosis was highlighted.[13] Specifically, the minimum GCL thickness indicates that the thinnest point in the GC-IPL analysis corresponds to the inner nasal sector; this sector was significantly reduced in our study but less significantly so than other sectors (Figs. 4, 5).

Due to the natural history of this disease, follow-up data on RNFL and GC-IPL thinning progression due to DOA are still missing in the literature; however, we can reasonably assume that the thinning process begins in the nasal GCL, in strict connection to the fovea, and progressively enlarges in the nasal area following a spiral pattern around the fovea: it reaches the temporal side and then enlarges in the peripheral areas of the macula. This process of RGC thinning in the macula has a specific pattern of deepening and enlargement (Fig. 6).[14] In the early stage of DOA (Fig. 6A), the last sectors involved are the external superior, temporal, and inferior and the internal superior, which correspond to the sectors with more preserved thickness (−25.2%, −30.2%, −27.9%, and −34.8%, respectively) compared with controls (Table 7, Fig. 5). In advanced stages of DOA (Fig. 6B), when all sectors appear evenly thinned, the internal superior sector is thicker than the others (−52.8% of reduction compared with controls) (Table 7).

A similar pattern of GC-IPL loss has been described for a different hereditary optic neuropathy: LHON.[15] In that study, the RNFL thinning occurred after the GC-IPL damage and began in the papillomacular bundle, corresponding to the temporal fibers, followed by the superior/inferior fibers and ending with nasal fiber involvement. These results are in agreement with recent evidence indicating that GC-IPL thickness is significantly correlated with visual recovery in patients with LHON who are treated with idebenone.[16]

Our study has several limitations. The number of patients was limited, as DOA is a rare disease, and a genotype–phenotype correlation is missing for the same reason. Visual function was assessed only through BCVA, not employing other parameters as visual field or electro-functional tests. Finally, the retrospective and cross-sectional nature of the study could have limited the strength of the results obtained.

In conclusion, we demonstrated a specific OCT biomarker in DOA progression for patients with early stages of disease or who are affected by advanced thinning of the GC-IPL. Furthermore, OCT biomarkers associated with visual outcomes in patients with DOA were identified. Topographical structural OCT metrics could be important in patient selection for future therapeutic trials for DOA.

Investigative Ophthalmology & Visual Science

Acknowledgments

The authors thank Leonardo Caporali, IRCCS Istituto delle Scienze Neurologiche di Bologna, Italy, for providing the *OPA-1* gene analysis.

Presented in part at the ARVO 2023 Annual Meeting, New Orleans, LA, April 23–27, 2023.

Disclosure: **M. Battista**, None; **C.P. Coutinho**, None; **A. Berni**, None; **E. Borrelli**, AbbVie (C), Apellis (C), Bayer Shering-Pharma (C), Hoffmann-La Roche (C), Zeiss (C); **A. Galzignato**, None; **G. Lari**, None; **L. Checchin**, None; **I.C. Pizza**, None; **L. Brotto**, None; **P. Nucci**, None; **F. Bandello**, Allergan (C), Bayer (C), Boehringer-Ingelheim (C), Fidia Sooft (C), Hoffmann-La Roche (C), Novartis (C), NTC Pharma (C), Sifi (C), Thrombogenics (C), Zeiss (C); **M.L. Cascavilla**, Chiesi Farmaceutici (F); **P. Barboni**, GenSight Biologics (C), Santhera Pharmaceuticals (F), Chiesi Farmaceutici (F), Omikron Italia (F)

References

1. Toomes C, Marchbank NJ, Mackey DA, et al. Spectrum, frequency and penetrance of *OPA1* mutations in dominant optic atrophy. *Hum Mol Genet*. 2001;10(13):1369–1378.
2. Alexander C, Votruba M, Pesch UE, et al. *OPA1*, encoding a dynamin-related GTPase, is mutated in autosomal dominant optic atrophy linked to chromosome 3q28. *Nat Genet*. 2000;26(2):211–215.
3. Eiberg H, Hansen L, Kjer B, et al. Autosomal dominant optic atrophy associated with hearing impairment and impaired glucose regulation caused by a missense mutation in the *WFS1* gene. *J Med Genet*. 2006;43(5):435–440.
4. Caporali L, Magri S, Legati A, et al. ATPase domain *AFG3L2* mutations alter OPA1 processing and cause optic neuropathy. *Ann Neurol*. 2020;88(1):18–32.
5. Jurkute N, Bertacchi M, Arno G, et al. Pathogenic *NR2F1* variants cause a developmental ocular phenotype recapitulated in a mutant mouse model. *Brain Commun*. 2021;3(3):fcab162.
6. Lenaers G, Reynier P, Elachouri G, et al. *OPA1* functions in mitochondria and dysfunctions in optic nerve. *Int J Biochem Cell Biol*. 2009;41(10):1866–1874.
7. Lenaers G, Neutzner A, Le Dantec Y, et al. Dominant optic atrophy: culprit mitochondria in the optic nerve. *Prof Retin Eye Res*. 2021;83:100935.
8. Pan BX, Ross-Cisneros FN, Carelli V, et al. Mathematically modeling the involvement of axons in Leber's hereditary optic neuropathy. *Invest Ophthalmol Vis Sci*. 2012;53(12):7608–7617.
9. Carelli V, Ross-Cisneros FN, Sadun AA. Optic nerve degeneration and mitochondrial dysfunction: genetic and acquired optic neuropathies. *Neurochem Int*. 2002;40(6):573–584.
10. Barboni P, Savini G, Cascavilla ML, et al. Early macular retinal ganglion cell loss in dominant optic atrophy: genotype-phenotype correlation. *Am J Ophthalmol*. 2014;158(3):628–636.e3.
11. Barboni P, Savini G, Parisi V, et al. Retinal nerve fiber layer thickness in dominant optic atrophy: measurements by optical coherence tomography and correlation with age. *Ophthalmology*. 2011;118(10):2076–2080.
12. Rönnbäck C, Milea D, Larsen M. Imaging of the macula indicates early completion of structural deficit in autosomal-dominant optic atrophy. *Ophthalmology*. 2013;120(12):2672–2677.
13. Zeng K, Chou B, Sadun AA. Minimum ganglion cell layer thickness is the best structural predictor of visual function in leber hereditary optic neuropathy. *Med Res Arch*. 2023;11(7). [online].
14. Asanad S, Tian JJ, Frousiakis S, et al. Optical coherence tomography of the retinal ganglion cell complex in Leber's hereditary optic neuropathy and dominant optic atrophy. *Curr Eye Res*. 2019;44(6):638–644.
15. Balducci N, Savini G, Cascavilla ML, et al. Macular nerve fibre and ganglion cell layer changes in acute Leber's hereditary optic neuropathy. *Br J Ophthalmol*. 2016;100(9):1232–1237.
16. Borrelli E, Berni A, Cascavilla ML, et al. Visual outcomes and optical coherence tomography biomarkers of vision improvement in patients with Leber hereditary optic neuropathy treated with idebenone. *Am J Ophthalmol*. 2023;247:35–41.